Research on Engineering Structures & Materials
www.jresm.org
MIM Research Group

Research Article

Stress analysis of aircraft tow hook using non-destructive testing techniques and numerical simulation

Ömer Kurt [1,a], Mesut Uyaner [*,2,b]

[1]*The Graduate School of Natural and Applied Sciences, Necmettin Erbakan University, Konya, Türkiye*
[2]*Department of Aeronautical Engineering, Faculty of Aeronautics and Astronautics, Necmettin Erbakan University, Konya, Türkiye*

Article Info

Article History:

Received 03 Sep 2025
Accepted 26 Jan 2026

Keywords:

Aircraft tow hook;
Non-destructive testing techniques;
AISI 4130 alloy steel;
Finite Element Method;
Stress analysis;
Safety factor

Abstract

Non-destructive testing was applied to an aircraft tow hook made of forged AISI 4130 alloy steels to evaluate its structural integrity under service conditions. Five inspection methods including magnetic particle, liquid penetrant, eddy current, ultrasonic, and radiographic testing were applied to the same component and correlated with finite element stress analysis. Eddy current, ultrasonic, and radiographic methods proved ineffective due to material ferromagnetism, complex geometry, and field equipment limitations, while liquid penetrant testing detected surface indications but suffered from a high level of non-relevant responses. In contrast, magnetic particle testing reliably identified a linear surface crack approximately 13 mm long at the inner curvature near the attachment region. Finite element analysis indicated a yield utilization of approximately 43%, corresponding to a safety factor of about 2.3 under nominal towing loads, and fracture-mechanics evaluation yielded a critical crack length of 19.6 mm, indicating that the observed defect had reached about 66% of the critical value. The strong agreement between experimental crack detection and numerical stress predictions demonstrates the value of integrating targeted NDT with finite element analysis and confirms magnetic particle testing as the most reliable inspection method for forged AISI 4130 aircraft tow hooks under realistic field conditions.

1. Introduction

Aircraft ground handling includes towing operations in which the tow hook must safely withstand operational forces to prevent structural failure [1]. If a tow hook fractures or fails under load, the aircraft cannot be moved and may suffer Foreign Object Damage from debris, potentially leading to serious incidents [2,3]. Therefore, maintaining the integrity of tow hooks through proper design, material selection, and routine inspections is essential for flight safety [4,5]. Aviation authorities emphasize that ground equipment like tow bars and tow hooks receive regular maintenance and non-destructive inspections to prevent costly accidents [5,6].

Numerous studies have highlighted the importance of non-destructive testing (NDT) techniques in the aviation industry. For instance, Ulus et al. surveyed common NDT methods used in aircraft maintenance and showed their effectiveness in detecting surface cracks on airframe components [7]. Demircioğlu et al. focused on composites and demonstrated how methods like ultrasonic and radiographic inspection can reveal subsurface flaws in complex materials [8]. Ibrishev et al. emphasized that although effective NDT techniques are available for finished products, repairing

*Corresponding author: muyaner@erbakan.edu.tr
[a]orcid.org/0009-0006-4200-2030; [b]orcid.org/0000-0003-2743-2340
DOI: http://dx.doi.org/10.17515/resm2026-1133me0903rs

damage that occurs during aircraft operation remains complex [9]. Broader reviews by Gupta et al. and Rao document advances in NDT technology and applications, underscoring that timely detection of cracks or damage can avert failures in service [10,11]. In particular, magnetic particle and liquid penetrant inspections are noted for their success in identifying fine surface discontinuities in steel parts [12]. Magnetic particle testing is widely used to detect surface and near-surface cracks in ferromagnetic materials [13]. It is an essential, highly sensitive, and user-friendly non-destructive technique for such applications [14]. On the numerical side, the Finite Element Method (FEM) has become a powerful tool for stress analysis of mechanical and aerospace components. Petrici et al. used FEM to obtain the stress and strain field in the towbar and the towing system. The experimental tests validate the theoretical results obtained [15]. In the context of vehicle and aircraft hardware, FEM-based studies have been conducted on towing assemblies and related parts. For instance, Aftab et al. developed a numerical model for a Boeing 737 nose landing gear to ensure its structural safety under operational loads [16]. Yadav et al. used structural finite element analysis (FEA) to analyze the nose gear's stress behavior and displacement during landing, as well as to assess the effect of the runway gradient [17]. More recently, Lin et al. combined finite element simulations with experimental modal testing for a B-727 aircraft nose landing gear, evaluating its strength and vibration performance during towing operations [18]. These works show the state-of-the-art in experimental NDT and computational analysis; however, most studies treat these approaches separately. There is a research gap in integrating multiple NDT methods with FEM for the same component to cross-verify findings. While some attempts at validation of experimental results with modelling exist in other fields [19], in aerospace components such combined studies are scarce. This gap is critical: a unified approach could improve defect detection and structural assessment by leveraging the strengths of both NDT and FEM.

In light of the above, the present work provides an integrated evaluation of an aircraft tow hook using five different NDT techniques in conjunction with finite element stress analysis. This dual approach is novel, as previous literature has not extensively reported correlating NDT findings with FEM predictions for towing hardware. By comparing experimental NDT results with simulation, the study identifies critical stress regions and verifies whether detected discontinuities align with high-stress zones – an important cross-check that enhances confidence in the findings. Unlike prior works that might focus only on a single NDT method or purely on analysis, this study uses a comprehensive suite (magnetic particle, liquid penetrant, eddy current, ultrasonic, and radiographic testing) on the same component, providing a broad assessment of each method's effectiveness. The key outcomes, including the superior crack-detection capability of magnetic particle testing and the FEM-calculated safety factor of the tow hook, fill the knowledge gap by demonstrating how numerical simulation can validate and complement NDT in identifying potential failure points. In comparison to similar studies, our results show agreement in general trends (e.g., known sensitivity of magnetic particle tests [13]) but also highlight where certain methods (ultrasonic, radiography) may fall short on complex geometries – a nuance not thoroughly documented before for tow hooks. The scientific contribution of this work lies in this holistic inspection methodology. It provides aviation maintenance engineers with a validated inspection strategy: focusing on the most sensitive NDT method for the given material and geometry, and using FEM as a diagnostic tool to interpret and reinforce the experimental observations. Ultimately, the findings of this study can contribute to the development of more reliable tow hook inspection routines and inform design improvements, thereby enhancing safety margins and reducing the risk of towing-related incidents.

2. Materials and Methodology

2.1 Material Properties

Forged components made of AISI 4130 alloy steel are widely used in the oil and gas, aerospace, agricultural, and defense industries, where reliable strength and toughness are required. Typical applications include forged valve bodies, pumps, and other medium- to low-stress structural parts. Fig. 1 shows the aircraft tow hook examined in this study, which was manufactured from AISI 4130 steel by hot forging at approximately 1000 °C. After forging, the hooks were oil-quenched from 850

°C and subsequently double-tempered at 560 °C and 530 °C, respectively, to achieve a balanced combination of strength and ductility.

Fig. 1. Aircraft tow hook

The typical mechanical properties of the heat-treated AISI 4130 alloy steel used in this study are presented in Table 1.

Table 1. Mechanical properties of AISI 4130 steel [20,21]

Property	Value	Unit
Yield strength	630	MPa
Ultimate tensile strength	800	MPa
Hardness	380	HV
Young's modulus	205	GPa
Poisson's ratio	0.29	–
Density	7.85	g/cm^3
Fracture toughness	75	$MPa{\cdot}m^{1/2}$

According to Linear Elastic Fracture Mechanics (LEFM), the critical crack length for AISI 4130 can be determined using Eq (1) [22].

$$K_I = Y\,\sigma\,\sqrt{\pi a} \Rightarrow a_c = \frac{1}{\pi}\left(\frac{K_{IC}}{Y\,\sigma}\right)^2 \quad (1)$$

where, K: Stress intensity factor, σ: Applied normal stress, a: Crack length, Y: Geometry factor, a_c: Critical crack length, K_{IC}: Fracture toughness

For a conservative estimation, the crack observed on the tow hook can be assumed to behave as an edge or surface crack in a wide plate. Under this assumption, the geometry factor Y is taken as 1.12. For the maximum stress of 270 MPa obtained in this study, the corresponding critical crack length is calculated to be 19.6 mm. To account for uncertainty in crack geometry and depth, a brief sensitivity consideration was conducted by varying the geometry factor within a reasonable range ($Y = 1.0–1.25$), consistent with shallow-to-moderate surface crack configurations reported in the literature. This variation yields a critical crack length range of approximately 17.5–22 mm. Within this range, the experimentally observed crack length of approximately 13 mm corresponds to about 60–75% of the critical value, confirming that the crack has progressed significantly toward instability even under conservative assumptions.

It should be noted that magnetic particle inspection provides reliable information on surface crack length, while the crack depth and exact crack shape cannot be directly determined using this method. Therefore, the fracture-mechanics evaluation presented here is intended as a screening-level assessment, based on a conservative surface-crack assumption. The objective of this analysis is not to predict the exact remaining life, but to evaluate whether the detected crack length approaches a critical threshold under nominal towing loads.

2.2. Research Methodology

The methodology combines standardized non-destructive testing (NDT) on the actual part with finite element method (FEM) on a geometrically accurate model under towing loads. After material/property confirmation (Table 1), five NDT methods were applied per Table 2, then results were compared with ANSYS-based stress/deformation maps to confirm whether indications align with predicted hot-spots. Using complementary methods mitigates false negatives from any single technique; FEM supplies a physics-based expectation of crack-prone zones to guide interpretation and future inspections. The brands and models of the test devices used in this study and the standards followed for each test are summarized in Table 2.

Table 2. Testing devices and relevant standards

Non-destructive testing method	Standards	Test device brand and model
Magnetic particle	ISO 9934-1/2/3, ISO 3059, ASTM-E1444	Magnaflux ZA-1633
Ultrasonic	ISO 17640, 16809, EN 12668-1	Eddyfi Panther 2/Mantis/Cypher
Liquid penetrant	ISO 3452-1, ISO 3059	Magnaflux ZA-28/37/915
Radiographic	ISO 17636-1/2, 19232	TroyMet
Eddy current	ISO 17643	Olympus ECT systems

2.2.1 Eddy Current Testing

Eddy current testing was performed using a surface probe with a differential ferrite core in accordance with ISO 17643. 100 kHz was selected as the nominal operating frequency due to the ferromagnetic nature of AISI 4130 steel. Under typical inspection conditions, DC pre-magnetization is applied to stabilize magnetic permeability and improve signal-to-noise ratio; however, the required equipment was not available in the present study, and the inspection was therefore conducted without pre-magnetization. Calibration was performed using an AISI 4130 reference block containing 0.5, 1.0, and 2.0 mm electrical-discharge machining notches, and the amplitude and phase responses were verified across the frequency sweep. This configuration was selected due to known limitations of eddy current testing in ferromagnetic steels.

2.2.2 Ultrasonic Testing

Ultrasonic testing was performed under the best achievable field conditions permitted by the available equipment. Ultrasonic testing was conducted using a portable flaw detector equipped with a 5 MHz straight-beam longitudinal-wave contact probe with a 10 mm active diameter. Calibration was performed on a steel reference block containing side-drilled holes in accordance with ISO 17640 and EN 12668-1. A glycerin-based couplant was applied to ensure acoustic coupling, and the inspection gate was set from the surface echo to a sound-path depth of 60 mm.

Despite proper calibration and parameter control, the complex curved geometry and variable cross-section of the forged tow hook caused beam distortion, multiple internal reflections, and poor signal-to-noise ratio. Advanced ultrasonic configurations such as phased-array, immersion testing, or custom angle-beam wedges were not available at the test facility. Under these practical conditions, conventional straight-beam ultrasonic testing did not yield interpretable flaw indications and was therefore deemed unsuitable for reliable inspection of this component.

2.2.3 Radiographic Testing

Radiographic inspection was performed in accordance with ISO 17636-1:2021 (film technique for metallic materials) and ISO 19232 (IQI classification). The TroyMet industrial X-ray unit (tungsten target, constant potential) was operated at the parameters with their values are shown in Table 3.

The film type used in the radiographic test was AGFA D7 (Class C, medium-speed, EN 584-1), used together with 0.03-mm lead intensifying screens placed on both the front and back sides. Processing was performed under red-safe light using manual developer and fixer cycles, including 5 minutes of development, followed by fixing, washing, and drying. A Type 2 ISO 19232-1 IQI (wire type, Fe) was placed on the source side; the smallest visible wire was No. 10 (1.0 mm), giving a basic IQI sensitivity of 2 %. The processed film is then examined on a light inspection panel.

Table 3. Values of parameters for radiographic testing

Parameters	Current	Duration	Voltage	Application Distance	Focal-spot size
Test Values	4 mA	90 s	200 kV	915 mm	2 mm

2.2.4 Liquid Penetrant Testing

Fluorescent penetrant inspection was conducted in accordance with ISO 3452-1:2021 and ISO 3059. A post-emulsifiable fluorescent penetrant system comprising Magnaflux ZL-37 penetrant, ZE-4B emulsifier, and ZP-9F non-aqueous wet developer was used. Prior to testing, the surface was cleaned with the SKC-S solvent cleaner and air-dried. The penetrant was applied and allowed to dwell for 20 ± 2 minutes at 22 ± 3 °C. Excess penetrant was removed by post-emulsification for 60 seconds, followed by rinsing with a low-pressure water spray (< 0.35 MPa, 25–40 °C). The component was then dried using hot air at 50 ± 5 °C for 5 minutes. The developer was subsequently applied to achieve a coating thickness of 0.02–0.05 mm, and a developer dwell time of 10 minutes was observed. Inspection was performed under UV-A illumination at 365 nm with an intensity greater than 1000 μW/cm^2 at a distance of 38 cm, while ensuring that ambient white-light levels remained below 20 lx, as specified in ISO 3059. System sensitivity was verified using a Type 1 NiCr cracked reference panel (JIS K C-1 equivalent) before examination.

2.2.5 Magnetic Particle Testing

Magnetic particle testing was selected due to its high sensitivity to surface and near-surface discontinuities in ferromagnetic steels. Following the previous four tests, a magnetic particle test was performed, the method recommended by the manufacturer.

Prior to testing, the hook was thoroughly cleaned to remove all grease and contaminants. The main purpose of this cleaning was to prevent any residual substances from concealing potential discontinuities. It was then positioned within a device equipped with a five-turn coil (Fig. 2).

Fig. 2. Aircraft tow hook sample washing with magnetic particle testing solution

Magnetic particle inspection was performed according to ASTM E1444/E1444M-25 and ISO 9934-1/-3 using a Magnaflux ZA-1633 wet horizontal bench unit. The tow hook was magnetized circularly by-passing current through a five-turn coil, inducing circumferential fields across the hook section. ASTM-E1444 refers to ASTM-E709-21 for calculation. The magnetizing current was calculated utilizing Eq (2) [23].

$$NI = \frac{K}{L/D} \tag{2}$$

Where, N: Number of turns in the coil, I: Coil current to be used, K: Empirically derived constant, L: Part length, D: Part diameter, NI: Ampere-turns.

The calculation is provided to document compliance with ASTM E1444 requirements; it does not represent a parametric optimization but ensures adequate magnetization under field conditions. K values in Eq. (2) have three options as presented in Table 4. The ampere-turns and ampere values generated for N=5 and length-to-diameter ratio (L/D) of 5. The tow hook cross-section is <0.1 of the coil area (Table 4, Option 1), so the highest K ensures adequate field strength and flaw visibility; lower K values are intended for larger parts occupying more of the coil.

Table 4. K values related to part cross-sectional area and coil cross-section

Option	Part cross-sectional area	K value	NI	I
1	< 0.1 of coil cross-section	45000	9000	1800
2	(> 0.1 and < 0.5) of coil cross-section	43000	8600	1720
3	< 0.5 of coil cross-section	35000	7000	1400

A fluorescent wet suspension (Magnaflux 14A in Carrier II oil) was used at 1.2 g/L ± 0.2 g/L particle concentration, verified daily with a centrifuge tube test per ISO 9934-2. The bath was continuously agitated and maintained at 25 ± 3 °C. Field adequacy was confirmed using Type QQI shims (Quantitative Quality Indicators, 0.004 in) placed on flat zones of the hook and with a digital gaussmeter, verifying surface field strength between 2.0–3.5 mT (20–35 G) at magnetization.

Fluorescent inspection was conducted in a darkroom with UV-A intensity > 1000 μW cm^{-2} at 38 cm and ambient white light < 20 lx, complying with ISO 3059. After inspection, the tow hook was demagnetized by gradually reducing AC coil current from 1800 A to 0 A while moving the part axially through the field. Residual magnetism was checked (< 0.5 G) with a gaussmeter before re-oiling the surface.

2.2.6 Towing Force

During aircraft towing, the tow bar exerts a horizontal force on the tow hook that must overcome the rolling resistance of the aircraft. To estimate this towing force, the resistance was modeled using friction coefficients corresponding to different ground surfaces. Typical friction coefficients (μ) for runways are given in Table 5.

Table 5. Friction coefficients of different materials [24,25]

Material	Friction coefficient (μ)
Concrete runway	0.02–0.05
Asphalt runway	0.03–0.06
Grass/soil	0.1–0.2

During towing, aircraft weight and fuel load are critical; heavier loads and excessive towing speed increase the risk of accidents. Safe towing requires controlled speed and adherence to FAA guidelines [4]. The General Dynamics F-16 Fighting Falcon was considered in full configuration [26]. Standard ground-handling procedures recommend that the towing speed does not exceed approximately 10 km/h. Under such controlled conditions, towing is performed in a quasi-steady manner, and sudden acceleration or deceleration events are intentionally avoided. Consequently, the forces associated with starting and stopping were neglected in the present analysis. Assuming a constant towing velocity, dynamic inertial effects were not considered, and at these low operating speeds aerodynamic drag forces are negligible. Similar assumptions have been reported by Lin and Yang (2024), who analyzed commercial aircraft nose landing gear under towing (taxi-out) conditions and concluded that, for towing speeds on the order of 10 km/h, the influence of dynamic effects is negligible [18].

Nevertheless, it is acknowledged that real towing operations may involve minor transient effects such as gentle braking, turning maneuvers, small impacts, or slight misalignment between the tow bar and the aircraft. These effects may cause short-term load amplification beyond the nominal straight-tow condition considered here. From an engineering assessment perspective, the static towing force adopted in this study should be interpreted as a conservative baseline load, suitable for assessing structural robustness and correlating experimentally observed damage with numerically predicted stress concentrations.

The aircraft being serviced via the tow hook was analyzed in two weight configurations: empty (basic operating weight) and fuel-loaded (maximum taxi weight). The parameters used in the towing-force calculations are presented in Table 6, and all computations were performed assuming an asphalt surface. The angular position (θ) between tow hook and ground is illustrated in Fig. 3.

Table 6. Parameters of towing force calculations

Parameter	Value
Empty aircraft mass (m)	12,473 kg
Fuel-loaded aircraft mass (m)	19,187 kg
Average friction coefficient of asphalt runway (μ)	0.04

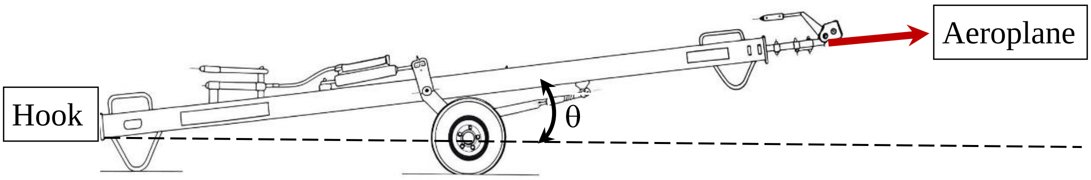

Fig. 3. Angular position of tow hook relative to ground

2.2.7 Numerical Analysis

The finite element analysis was conducted using ANSYS Mechanical. Boundary conditions were defined with fixed supports at the connection points and applied towing loads in the forward direction. Although the tow hook is mechanically connected through a pin–clevis joint, complete rotational freedom is not realized in practice due to contact friction, load-induced constraint, and manufacturing tolerances. To evaluate the influence of this modeling assumption and to avoid bias associated with an arbitrary boundary definition, a simplified parametric comparison was conducted between a fully fixed support and a rotationally released support condition. The fixed support produced stress values approximately 10–15% higher than the released case at the critical region. Therefore, the fixed boundary condition adopted in this study represents a conservative upper-bound estimate of stress, ensuring that the reported results do not underestimate the structural demand and improving the reproducibility of the analysis under realistic field conditions. Load magnitudes were calculated based on aircraft weight conditions (empty and fuel-loaded).

According to Fig. 4, the mesh was refined up to approximately 700,000 elements, after which the maximum equivalent stress stabilized at around 160 MPa, indicating that further mesh refinement had a negligible effect on the stress results. In the structural analysis of the tow hook, a three-dimensional mesh model consisting entirely of tetrahedral elements was generated using the finite element method (FEM). Tetrahedral elements are widely preferred in such analyses due to their high adaptability to complex geometries and compatibility with automatic meshing algorithms. During the modelling process, a high-resolution mesh was constructed, and the geometric quality of each element was evaluated using the element quality parameter. Element quality, which represents the overall distortion of an element relative to its ideal finite element shape, is a critical indicator of mesh performance and has a significant influence on the accuracy and stability of numerical solutions.

The mesh quality analysis revealed that the element quality values ranged between 0.2132 and 1, as shown in Fig. 5. The majority of the elements exhibited quality values between 0.4 and 0.7, indicating that the overall mesh maintained an acceptable level of accuracy for numerical computation. Locally lower element quality values (approaching 0.2) were observed in the regions with complex geometry and tight curvature, particularly near the inner fillets and hook transitions. Although these areas may slightly reduce local solution accuracy due to geometric complexity, the limited extent of such elements ensures that the global model accuracy remains within acceptable limits.

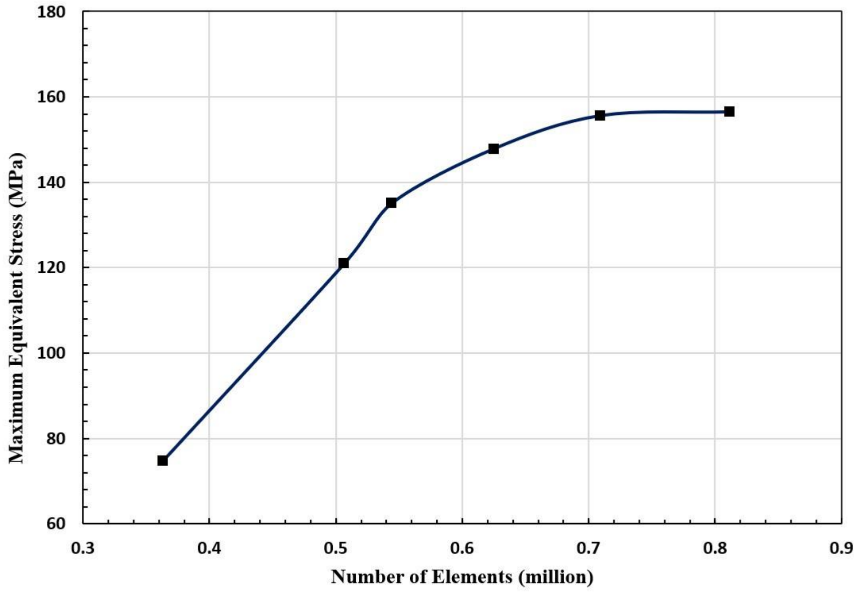

Fig. 4. Mesh convergence study

Visual evaluations based on color contour maps (Fig. 5) clearly demonstrated the spatial distribution of element quality. In the mesh quality plot, blue and green zones represent elements with high quality values (0.6–0.9), which dominate most regions of the model. Conversely, yellow to red zones, indicating lower element quality (below 0.4), were confined to limited areas, mainly around the inner fillets and sharp curvature transitions. This distribution confirms that the overall mesh exhibits high numerical quality with well-shaped tetrahedral elements. Particularly at load application points and structurally critical regions, the element transitions were smooth, minimizing geometric distortion and improving both the stability and accuracy of the analysis results.

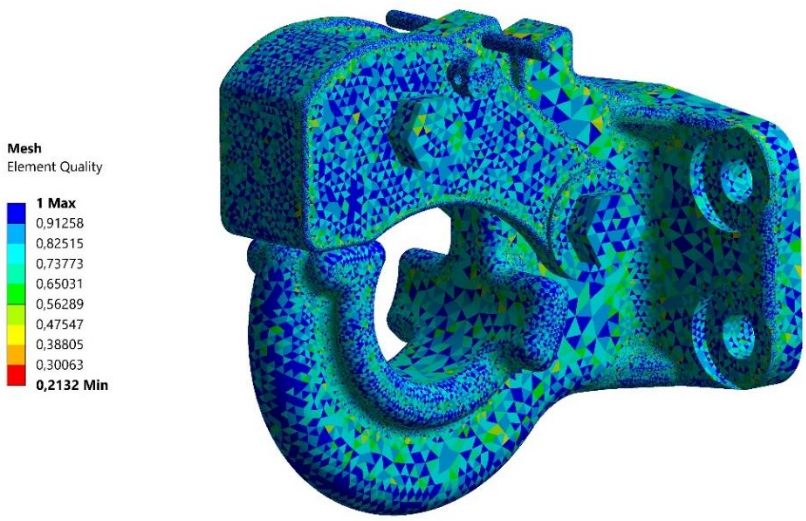

Fig. 5. Distribution of element quality values of tow hook

In conclusion, the tetrahedral mesh structure applied in the structural analysis of the tow hook, a geometrically complex mechanical component, provides both numerical accuracy and engineering reliability. The homogeneous distribution of element quality values and the low distortion levels in critical regions demonstrate that the mesh employed offers an effective and robust basis for FEM-based structural analysis. Fig. 6. illustrates the research methodology, including material characterization, application of five NDT methods on the tow hook, analysis of NDT results, finite element simulation of the tow hook under towing loads, and correlation of the experimental and numerical findings. It provides a visual overview of all steps in this methodology, from initial inspections to final analysis.

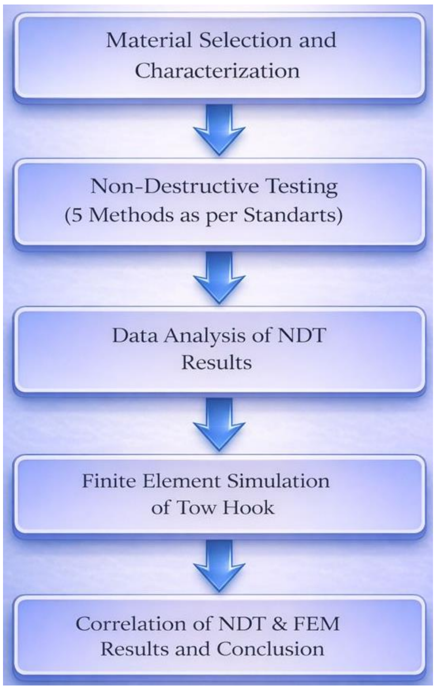

Fig. 6. The research methodology

3. Results and Discussion

3.1. Results

A total of five different tests were performed to investigate the damage analysis of the tow hook. The findings from these tests yielded highly informative results. Reviewing the outcomes of each test individually provides valuable insight.

3.1.1 Eddy Current Test

The tested tow hook is ferromagnetic in nature. Compared to non-ferromagnetic materials, the magnetic permeability of ferromagnetic materials varies depending on their internal position, which may adversely affect the signal-to-noise ratio. It is widely accepted that the use of a DC magnetization technique–where magnetization is partially or fully directed in one orientation–in combination with eddy current testing ensures reliable inspection [27]. This necessitates that the material reaches magnetic saturation before testing [28]. However, while this may appear effective theoretically, it is rarely preferred in practice. This is primarily because, even if the material is brought to magnetic saturation, its residual magnetism is short-lived and easily influenced by even minor magnetic fields. For instance, the Earth’s magnetic field itself can have an impact on the material. As the testing facility lacked the equipment required for pre-magnetization, the eddy current test was performed without this step. No interpretable eddy current indications were obtained under the available inspection conditions.

3.1.2 Ultrasonic Test

Preliminary visual inspection indicated that the complex curved geometry and uneven surface condition of the tow hook posed challenges for reliable ultrasonic inspection using conventional straight-beam techniques. In stressed metallic components, ultrasonic wave propagation may exhibit non-linear behavior due to interactions with dislocation structures, leading to waveform distortion and degraded echo interpretation [29].

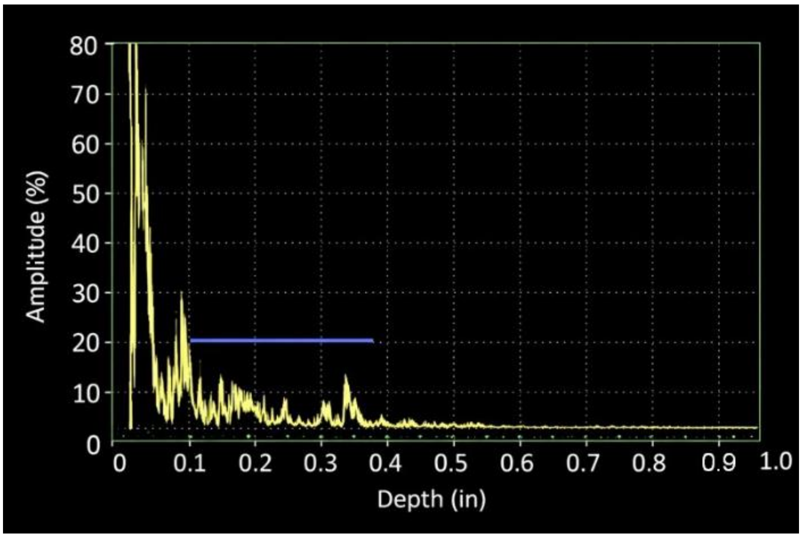

Fig. 7. Ultrasonic A-scan showing geometry-induced reflections and low signal-to-noise ratio (estimated SNR ≈ 3–4 dB)

As illustrated in Fig. 7, the ultrasonic A-scan is characterized by multiple overlapping reflections, with the back-wall echo amplitude comparable to the background noise level. The signal-to-noise ratio (SNR), estimated by comparing the peak back-wall echo amplitude to the mean background noise within the inspection gate, did not exceed approximately 3–4 dB across multiple probe positions. This value is below the commonly accepted threshold (≥6 dB) required for reliable flaw detection in conventional ultrasonic testing. Reflections from internal curvature further overlapped with back-wall echoes, preventing definition of a meaningful detection limit; consequently, the effective minimum detectable flaw size was conservatively assumed to exceed 3–4 mm for surface-connected discontinuities.

Ultrasonic inspection performance is strongly influenced by the compatibility between probe size, geometry, and the inspected material [30], and the technique exhibits limited sensitivity to surface-connected flaws when used as a standalone method [31]. Despite proper calibration, controlled couplant application, and optimized gate settings in accordance with relevant standards, the recorded signals were dominated by geometry-induced mode conversions and surface-scatter noise. Under these practical field conditions, conventional single-element straight-beam ultrasonic testing did not yield interpretable indications and was therefore deemed unsuitable for reliable inspection of the examined tow hook in the absence of advanced phased-array or immersion-based configurations.

3.1.3 Radiographic Test

As illustrated in Fig. 9, no interpretable discontinuities were identified on the radiographic film obtained under the applied exposure conditions. At an operating voltage of 200 kV, X-ray penetration through the 22 mm thick quenched-and-tempered AISI 4130 steel approaches the upper limit of Class C film radiography. Even at maximum voltage, the resulting film density gradient remained low, with a mean optical density of approximately 1.4 ± 0.2.

Scatter radiation and geometric unsharpness, estimated to be approximately 1.8 mm at a source-to-film distance of 915 mm, further reduced image contrast and masked potential small planar flaws. Based on the applied exposure parameters (200 kV, AGFA D7 Class C film, and ISO wire-type

IQI), the achieved basic image quality indicator sensitivity was approximately 2%, corresponding to a minimum detectable thickness variation of about 0.4–0.5 mm in a 22 mm steel section. Under these conditions, planar cracks with an opening width below approximately 1.0 mm are considered undetectable.

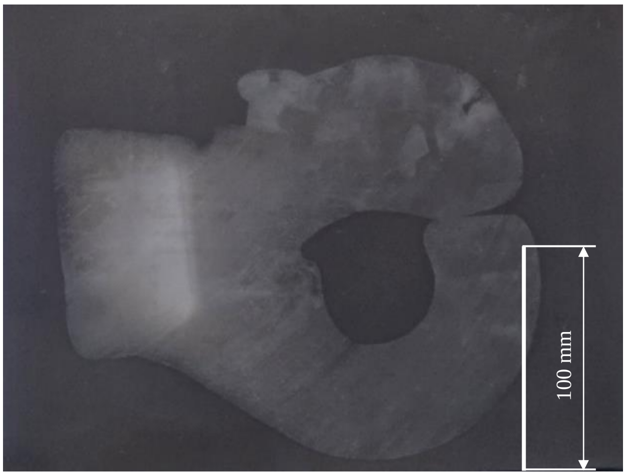

Fig. 8. Radiographic image of the aircraft tow hook

The absence of visible flaw indications in Fig. 9 is therefore attributed to the combined effects of material thickness, high density, and complex overlapping geometry, rather than insufficient inspection execution. Reliable crack detection for this component would require either higher-energy radiation sources (≥ 1 MeV X-ray or Co-60/Ir-192 γ-ray) or digital radiography with enhanced contrast resolution, which were not available under the present field conditions.

3.1.4 Liquid Penetrant Test

As shown in Fig. 10, fluorescent penetrant testing revealed both relevant and non-relevant surface indications on the forged tow hook. Linear or rounded indications conforming to ISO 23277 Level 2 criteria were classified as relevant, while isolated fluorescence below 1 mm and diffuse background responses were disregarded. Surface roughness associated with the forging process produced scattered fluorescence, which limited interpretability despite careful surface preparation. To mitigate this effect, oxide scale was removed by light abrasive polishing, post-wash pressure was reduced to prevent penetrant retention in surface pores, and an etched control coupon was processed concurrently to monitor background intensity. Nevertheless, diffuse non-relevant indications remained present.

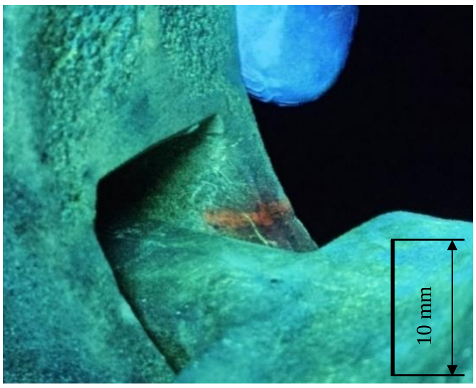

Fig. 9. Observed discontinuities after liquid penetrant testing

Quantitative evaluation showed an average false-indication density of approximately 6–8 non-relevant indications per 100 cm^2 outside the stress-critical regions, primarily associated with surface roughness and forging marks. In contrast, relevant linear indications were sparse and localized. This resulted in a low signal-to-background ratio, demonstrating that while fluorescent penetrant testing is sensitive to surface-connected discontinuities, its reliability is strongly dependent on surface finishing quality for forged steel components.

3.1.5 Magnetic Particle Test

Prior to inspection, a gaussmeter check confirmed the absence of residual magnetic field. The tow hook was then positioned within the test coil, and a current of 1,800 A was applied to induce magnetization, while a fluorescent magnetic particle suspension was uniformly applied. Adequate magnetization was verified by post-test gaussmeter readings, and inspection was conducted in a darkroom under UV-A illumination.

As illustrated in Fig. 11, a distinct linear indication with a measured length of approximately 13 mm was detected on the inner curvature near the attachment lug. The indication was documented using a calibrated scale and a 10 mm reference grid and exceeded ISO 23278 Level 2 acceptance criteria for critical hardware, leading to its classification as rejectable.

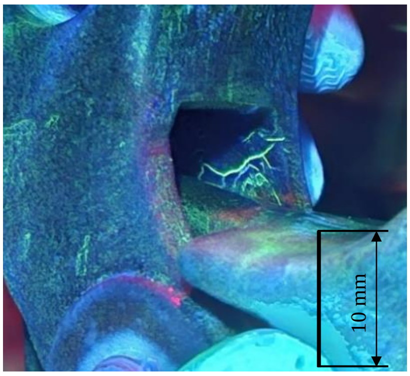

Fig. 10. Component inspected after magnetic particle test

No comparable linear indications were observed outside the stress-critical region predicted by the finite element analysis, indicating a low false-indication density. The indication was resolved with high contrast relative to the background particle distribution, resulting in a high signal-to-background ratio and confirming the superior sensitivity and specificity of magnetic particle testing for this component.

3.2. Discussion

3.2.1 Towing Force

During aircraft towing, the positioning and angle of the tow hook relative to the aircraft are of critical importance. The positioning directly affects the applied forces; incorrect alignment may shorten the service life of the component, cause material fatigue, or lead to undesired cracks and fractures. In the present scenario, the effects of the aircraft being either fuel-loaded or empty were evaluated in conjunction with the angular positioning of the hook. In practice, the angle between the two hook and ground ranges from 0° to 20°. Table 7 presents the calculated towing force values.

Table 7. Towing force values with ground angle θ

	Tow hook angle, θ	0°	10°	20°
Towing force [kN]	Empty	4.9	4.98	5.21
	Fuel-loaded	7.53	7.65	8.01

3.2.2 Deformation and Stress

The analysis results included total deformation, maximum principal stress, and von Mises stress distributions. Total deformation analysis demonstrates the vertical displacement resulting from the applied force. Fig. 11 indicates the region experiencing maximum deformation (red) corresponding to the highest stress concentration. Areas experiencing minimal deformation are indicated in blue. The affected regions remain consistent across all angular variations. The distribution of maximum principal stress obtained from the finite element analysis is shown in Fig. 12. The transition from blue to green towards red corresponds to increasing stress levels.

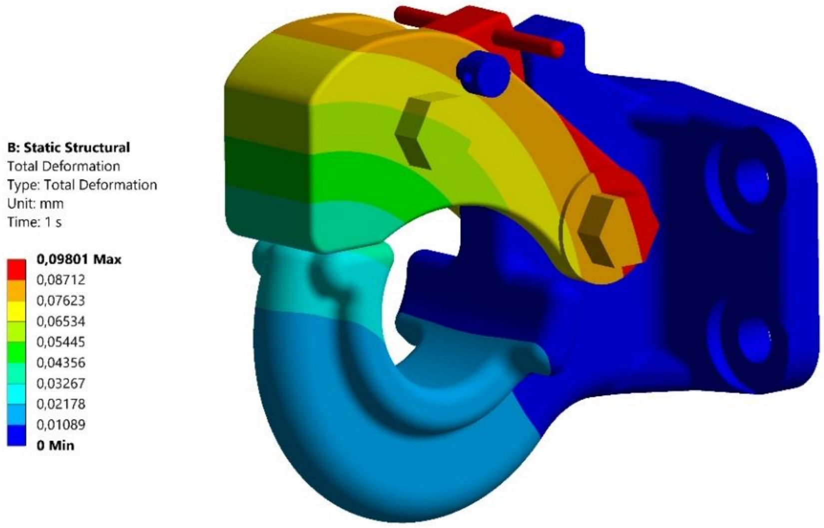

Fig. 11. Total deformation

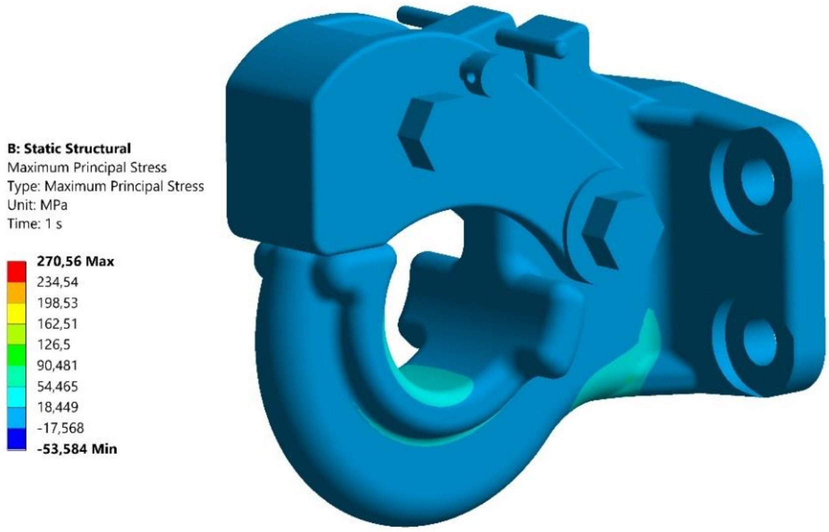

Fig. 12. Distribution of maximum principal stress in the aircraft tow hook under nominal towing loads

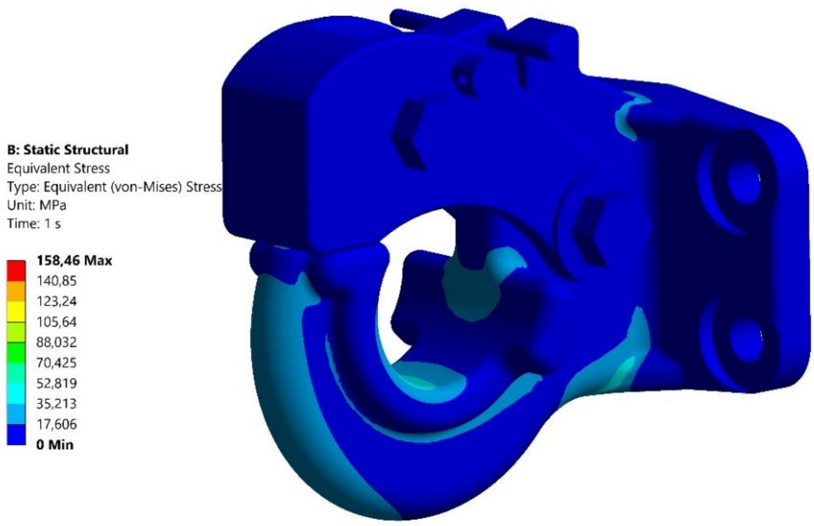

Fig. 13. Equivalent von mises stress

The identified high-stress regions correlate strongly with the cracks observed during non-destructive inspection, further supporting the structural assessment. For all angular variations, the analysis consistently revealed a localized high-stress concentration in the same region, indicating a potential failure zone. To quantify the stress level relative to material strength, a yield utilization ratio (UR) was defined as the ratio of the maximum principal stress obtained from the finite element analysis (σ_{max}) to the material yield strength (σ_y), i.e., UR = σ_{max} / σ_y. The corresponding safety factor was calculated as its reciprocal (SF = σ_y / σ_{max}).

The finite element analysis yielded a maximum principal stress of approximately 270 MPa, corresponding to a yield utilization ratio of UR ≈ 0.43 and a safety factor of approximately 2.3. Equivalent von mises stress analysis (Fig. 13) shows that stress is highest at the connection (end) section of the tow hook and lowest in the blue-colored regions. This aligns with the results obtained from the tests–particularly the indications observed in the liquid penetrant test (Fig. 9) and the distinct discontinuities revealed in the magnetic particle test (Fig. 10). The analysis confirms that the connection areas are the most susceptible to cracking or fracture.

3.2.3 Limitations of Non-Destructive Testing Methods

Several non-destructive testing methods, including eddy current, ultrasonic, and radiographic inspection, did not yield reliable flaw detection for the examined tow hook due to the combined effects of material properties, complex geometry, and practical equipment constraints. These outcomes emphasize that the effectiveness of an NDT method is highly dependent on its compatibility with the component geometry and available inspection configurations.

In particular, the limitations observed in ultrasonic testing did not arise from inadequate parameter control or non-compliance with standards, but from the inherent mismatch between the curved geometry of the tow hook and the conventional straight-beam UT setup employed. This clarification reconciles the controlled experimental methodology with the inconclusive inspection results.

3.2.4 Crack Criticality and Safety Margin Assessment

The fracture-mechanics assessment provides an important context for interpreting the detected magnetic particle indication. Given that crack depth information is not available from magnetic particle inspection, the present fracture-mechanics evaluation should be interpreted as a conservative screening tool rather than a detailed life-prediction model. From an engineering maintenance perspective, this level of assessment is sufficient to determine whether a detected surface crack has approached a critical condition requiring rejection or repair. More detailed crack-shape–dependent analyses would require advanced inspection techniques, which were beyond the scope of the present field-based study. Assuming a surface crack geometry with a geometry factor Y = 1.12, the critical crack length corresponding to the maximum principal stress of 270 MPa was calculated as 19.6 mm. The experimentally observed crack length of approximately 13 mm therefore corresponds to about 66% of the critical crack length under static towing conditions.

This comparison indicates that the detected crack has not yet reached the critical size for unstable fracture but has significantly reduced the remaining safety margin. A ±10% variation in the geometry factor (Y = 1.0–1.25) results in a critical crack length range of approximately 17.5–22 mm, which still places the observed crack within 60–75% of the critical threshold. From an engineering perspective, this proximity highlights the necessity of immediate rejection or repair, as further crack growth under cyclic towing loads could rapidly lead to fracture.

Although the global safety factor remains acceptable (SF ≈ 2.3), the corresponding yield utilization indicates that local crack growth can significantly reduce the remaining safety margin well before yielding occurs. The combined FEM stress analysis and fracture-mechanics evaluation therefore demonstrate that the tow hook operates with an acceptable global safety factor under nominal loading, while local crack growth can critically compromise structural integrity.

4. Conclusion

This study presented an integrated structural integrity assessment of an aircraft tow hook by combining multiple non-destructive testing techniques with finite element stress analysis and fracture-mechanics–based evaluation. Rather than focusing solely on defect detection, the work aimed to clarify the capabilities and limitations of commonly applied inspection methods when used on a forged, geometrically complex aerospace component operating under service-relevant loads.

Among the investigated inspection techniques, magnetic particle testing demonstrated the highest effectiveness in identifying surface-connected defects at critical locations. In contrast, eddy current, ultrasonic, and radiographic inspections were shown to be inherently limited by the component geometry, material characteristics, and available field configurations. Importantly, these limitations did not arise from inadequate test execution or parameter control, but from a fundamental incompatibility between the inspection methods and the physical characteristics of the tow hook. This distinction underscores the necessity of method selection based on component-specific constraints rather than generalized inspection capability.

The finite element analysis revealed a consistent high-stress concentration in the same region where the relevant magnetic particle indication was detected, confirming the structural relevance of the observed defect. Although the tow hook exhibits an acceptable global safety factor under nominal towing loads, the associated yield utilization highlights that stress-based margins alone do not fully capture the risk posed by localized damage. The fracture-mechanics–based assessment provided essential context by demonstrating that the detected surface crack occupies a substantial fraction of the critical crack size for unstable fracture, indicating that local damage can significantly erode the remaining safety margin well before yielding occurs.

From an engineering and maintenance perspective, these findings emphasize that reliance on global safety factors or nominal stress criteria may lead to non-conservative conclusions for towing hardware subjected to cyclic service conditions. The integration of magnetic particle inspection with finite element stress analysis and crack-criticality evaluation enables a more realistic assessment of serviceability and supports timely rejection or repair decisions before catastrophic failure. The fracture-based crack assessment presented in this study represents a conservative, inspection-driven screening approach, intended to support maintenance decision-making rather than detailed crack-growth prediction. Beyond the specific case of the tow hook, the methodology presented in this study is applicable to other forged aerospace components with complex geometry, where local damage mechanisms may govern structural integrity despite apparently adequate global design margins.

References

[1] IATA. Aircraft operational availability 2022: 1–47. https://www.iata.org/contentassets/bf8ca67c8bcd4358b3d004b0d6d0916f/aoa-2nded-2022.pdf (accessed October 7, 2025).

[2] Chauhan T, Goyal C, Kumari D, Thakur AK. A review on foreign object debris/damage (FOD) and its effects on aviation industry. In: Sakthivel S, Karthikeyan S, Palani A, editors. International Conference on Nanotechnology: Ideas, Innovation and Industries, vol. 33, Anna Univ, Syed Ammal Engn Coll, Ramanathapuram, INDIA: Materials Today: Proceedings, Elsevier Ltd.; 2020, p. 4336–4339. https://doi.org/10.1016/j.matpr.2020.07.457.

[3] Masniza Y, Zulfabli HM, Amarul T, Khairunnisa SN, Zilawati NARNN, Nazera D, et al. Potential FOD defects on the composite material. 5th International Conference on Green Design and Manufacture (IConGDM 2019), Jawa Barat, Indonesia: 2019, p. 020056. https://doi.org/10.1063/1.5118064.

[4] Federal Aviation Administration. Towbar and towbarless movement of aircraft. US Department of Transportation 2023: 1–16. https://www.faa.gov/documentLibrary/media/Advisory_Circular/AC_00-65A.pdf (accessed October 7, 2025).

[5] Federal Aviation Administration. ENR1. General rules and procedures. US Department of Transportation 2025. https://www.faa.gov/air_traffic/publications/atpubs/aip_html/part2_enr_section_1.1.html (accessed October 7, 2025).

[6] Yilmaz AA. Critical connections: network analysis of human errors in aviation accidents. The International Journal of Aerospace Psychology 2025; 35: 203–229. https://doi.org/10.1080/24721840.2025.2531741.

[7] Ulus Ö, Davarcı FE, Gültekin EE. Non-destructive testing methods commonly used in aviation. International Journal of Aeronautics and Astronautics 2024; 5: 10–22. https://doi.org/10.55212/ijaa.1418742.
[8] Demircioglu P, Seckin M, Seckin AC, Bogrekci I. Non-destructive testing methods in composite materials. In: Kumar A, Kumar Singla Y, R. Maughan M, editors. Fracture Behavior of Nanocomposites and Reinforced Laminate Structures, Cham: Springer Nature Switzerland; 2024, p. 487–516. https://doi.org/10.1007/978-3-031-68694-8_21.
[9] Ibrishev K, Prilipko E, Soldatkin M, Kononov N. Experimental research of quality of the adhesive repairs of composite structures using non-destructive testing. Research on Engineering Structures and Materials 2025; 11: 1051–1062. https://doi.org/10.17515/resm2024.351ma0712rs.
[10] Gupta M, Khan MA, Butola R, Singari RM. Advances in applications of non-destructive testing (NDT): a review. Advances in Materials and Processing Technologies 2022; 8: 2286–2307. https://doi.org/10.1080/2374068X.2021.1909332.
[11] Purna Chandra Rao B. Non-destructive testing and damage detection. In: Prasad NE, Wanhill RJH, editors. Aerospace Materials and Material Technologies, vol. 2, Springer; 2017, p. 209–228. https://doi.org/10.1007/978-981-10-2143-5_11.
[12] Jarvis R, Cawley P, Nagy PB. Performance evaluation of a magnetic field measurement NDE technique using a model assisted probability of detection framework. NDT & E International 2017; 91: 61–70. https://doi.org/10.1016/j.ndteint.2017.06.006.
[13] Sözeri V, Keskin O, Harmanşah C, Kozak İ, Kibar EN. Investigation of crack detection in magnetic particle testing images based on image process algorithms (in Turkish). Afyon Kocatepe University Journal of Sciences and Engineering 2023; 23: 115–122. https://doi.org/10.35414/akufemubid.1173473.
[14] Wu Q, Dong K, Qin X, Hu Z, Xiong X. Magnetic particle inspection: status, advances, and challenges – demands for automatic non-destructive testing. NDT & E International 2024; 143: 103030. https://doi.org/10.1016/j.ndteint.2023.103030.
[15] Petrici AV, Scutaru ML, Gheorghe V, Vlase S. Alternative solution for towing systems used in the automotive industry. Applied Sciences 2024; 14: 9131. https://doi.org/10.3390/app14199131.
[16] Aftab SG, Sirajuddin, Sreedhara B, Ganesh E, Babu NR, Aithal SK. Finite element analysis of a passenger aircraft landing gear for structural and fatigue safety. In: Ramesh MR, Dasarath S, Prashatha K, editors. 5th International Conference on Advanced Research in Mechanical, Materials and Manufacturing Engineering-2021, Elsevier; 2022, p. 152–158. https://doi.org/10.1016/j.matpr.2021.08.199.
[17] Yadav BK, Yadav R, Sudhakar K. Stress distribution analysis using ANSYS of the nose landing gear of STOL aircrafts considering runway gradient: a simulation study. Orchid Academia Siraha 2023; 2: 1–20. https://doi.org/10.3126/oas.v2i1.65618.
[18] Lin Q, Yang C, Bai Y, Qin J. Structural strength analysis and optimization of commercial aircraft nose landing gear under towing taxi-out conditions using finite element simulation and modal testing. Aerospace 2024; 11: 414. https://doi.org/10.3390/aerospace11050414.
[19] Chakravarti BJ, Rajasekhar K. Experimental investigation and modelling of the layered concrete with different proportions of steel fibers. Research on Engineering Structures and Materials 2025; 11: 957–968. https://doi.org/10.17515/resm2025-764me0316rs.
[20] Kurt Ö. Damage analysis of an aircraft tow hook (in Turkish). Master of Science. The Graduate School of Natural and Applied Science of Necmettin Erbakan University, 2025.
[21] ASM International Handbook Committee. Fracture Mechanics Properties of Carbon and Alloy Steels. Fatigue and Fracture, vol. 19, ASM International; 1996, p. 614–654. https://doi.org/10.31399/asm.hb.v19.a0002397.
[22] Jones DRH., Ashby MF. Engineering Materials 1: An Introduction to Properties, Applications and Design. 5th ed. Butterworth-Heinemann; 2019.
[23] ASTM–E709-21. Standard guide for magnetic particle testing. ASTM Volume 03.03: Nondestructive Testing (I): B548 – E2373, vol. 03.03, West Conshohocken, PA: ASTM International; 2021. https://doi.org/10.1520/E0709-21.
[24] Sofie M, Winiasri L, Triyono A. Planning for the extension of runway 01 for A330-200 aircraft type at Kalimarau Berau airport. Proceeding of International Conference of Advanced Transportation, Engineering, and Applied Social Science, vol. 3, 2024, p. 23–34.
[25] Wong JY. Theory of Ground Vehicles. Wiley; 2022. https://doi.org/10.1002/9781119719984.
[26] Bushell S, Willis D. Jane's All the World's Aircraft: In Service. JANES; 2025.
[27] Deng Z, Kang Y, Zhang J, Song K. Multi-source effect in magnetizing-based eddy current testing sensor for surface crack in ferromagnetic materials. Sens Actuators A Phys 2018; 271: 24–36. https://doi.org/10.1016/j.sna.2018.01.009.
[28] Jin X, Yang L. Research on eddy current-based detection method for pipeline hard spots. Measurement 2026; 257: 118952. https://doi.org/10.1016/j.measurement.2025.118952.

[29] Wang JJ, Wen ZX, Pei HQ, Gu SN, Zhang CJ, Yue ZF. Thermal damage evaluation of nickel-based superalloys based on ultrasonic nondestructive testing. Applied Acoustics 2021; 183: 108329. https://doi.org/10.1016/j.apacoust.2021.108329.

[30] Görgün E. Investigation of the effect of ultrasonic inspection probe diameters on impact echo value (in Turkish). Karadeniz Fen Bilimleri Dergisi 2022; 12: 381–389. https://doi.org/10.31466/kfbd.1077386.

[31] Sevim MA, Çelt AC, Kabar S, Akgünlü Ö. Applications of non-destructive testing methods on rails in railways (In Turkish). Demiryolu Mühendisliği 2020: 60–74. https://dergipark.org.tr/en/pub/demiryolu/issue/50417/658939